Received: 27 March 2021 | Revised: 6 May 2021 | Accepted: 18 May 2021

DOI: 10.1002/aoc.6320

RESEARCH ARTICLE

Applied Organometallic Chemistry WILEY

Rapidly, highly yielded and green synthesis of dihydrotetrazolo[1,5-*a*]pyrimidine derivatives in aqueous media using recoverable Pd (II) thiazole catalyst accelerated by ultrasonic: Computational studies

Mahmoud Abd El Aleem Ali Ali El-Remaily[1] | **Ahmed M. M. Soliman**[1] | **Mohamed E. Khalifa**[2] | **Nashwa M. El-Metwaly**[3,4] | **Amerah Alsoliemy**[3] | **Tarek El-Dabea**[1] | **Ahmed M. Abu-Dief**[1,5]

[1]Department of Chemistry, Faculty of Science, Sohag University, Sohag, Egypt

[2]Department of Chemistry, College of Science, Taif, Saudi Arabia

[3]Department of Chemistry, Faculty of Applied Science, Umm Al-Qura University, Makkah, Saudi Arabia

[4]Department of Chemistry, Faculty of Science, Mansoura University, Mansoura, Egypt

[5]Department of Chemistry, College of Science, Taibah University, Madinah, Saudi Arabia

Correspondence

Mahmoud Abd El Aleem Ali Ali El-Remaily, Department of Chemistry, Faculty of Science, Sohag University, 82524 Sohag, Egypt.
Email: mahmoud_ali@science.sohag.edu.eg; msremaily@yahoo.com

Nashwa M. El-Metwaly, Department of Chemistry, Faculty of Science, Mansoura University, Mansoura, Egypt.
Email: nmmohamed@uqu.edu.sa

Ahmed M. Abu-Dief, Department of Chemistry, College of Science, Taibah University, P.O. Box 344, Madinah, Saudi Arabia.
Email: amamohammed@taibahu.edu.sa; ahmed_benzoic@yahoo.com

Funding information

Taif University Researchers Supporting Project, Grant/Award Number: TURSP-2020/43

Here, we synthesized new thiazole complexes from Cu (II), Fe (III), and Pd (II) ions. Such complexes were characterized to present their chemical formulae, firstly. The octahedral geometry was suggested for the investigated complexes except Pd (II) complex (ARPTPd), which has a square-planer arrangement. ARPTPd was planned to be used as a catalyst for synthesis of dihydrotetrazolo[1,5-*a*]pyrimidine derivatives at mild conditions. The catalytic activity of ARPTPd complex in four-components reaction approach was deliberately monitored till it reaches the most favorable conditions. The advantages of suggested catalyst were basically summarized by using green solvent (H_2O), lower reaction time, and high products yields. Also, the superiority of ARPTPd complex and ultrasonic irradiation towards synthesis of dihydrotetrazolo[1,5-*a*]pyrimidine derivatives was revealed compared with other Lewis acids, basic, and ionic liquid catalysts. Furthermore, the mildness of conversion and compatibility with different functional groups makes it attractive. In addition, in consecration, computational aspects were often taken according to their effect on the declaration or discrimination of variable functional characteristics. Crystal packing systems of complexes were configured to extract important surface properties. DFT study was also applied to explain the causes behind the superiorly of ARPTPd complex. Also, the optimization process for intermediates was executed to support the suggested mechanism. Finally, this simple, economical, and green catalytic procedure may be applied to the industry in future.

KEYWORDS

DFT, recoverable catalyst, tetrazolopyrimidine derivatives, thiazole complexes, ultrasonic irradiation

1 | INTRODUCTION

Under mild conditions that otherwise require strict pressure and temperature conditions, the ultrasonic state increases the rate of organic transformation.[1] Ultrasonic irradiation is often used to promote different synthetic reactions through the creation, rising, and implosive collapse of bubbles in a liquid.[2] High pressures, extreme local heating, and a very short service life are created by the collapse of the bubbles initiated by cavitation. Cavitation functions as a way of focusing the diffuse energy of sound.[3] Ultrasonic irradiation is capable of triggering several reactions by supplying activation energy in the microenvironment, compared with traditional heating that supplies thermal energy in the macrosystem.[4] In addition, the other benefits of ultrasonic irradiation are high product yield, fast reaction times, minimization of by-products,[5] non-toxic and environmentally friendly solvents,[6] and energy saving.

Variable features were remarked regarding biological activity for heterocycles azo-category. As reported previously, few conventional and progressive one-pot synthesis strategy for heterocyclic tetrazolo [1,5-*a*]pyrimidine derivatives was investigated.[7–12] Due to their structural similarity to heterocyclic DNA and RNA bases, azolo-annulated pyrimidines and 1,2,4-triazines have attracted continuing interest. Consequently, these compounds can serve as biologically efficient antimetabolites. Azolo [1,5-*a*]pyrimidines are known as structural analogs of DNA and RNA purine bases.[13] As an anti-HBV (hepatitis B virus),[14] antitumor,[15] and anticancer agents,[16] substituted tetrazolo pyrimidine are used as well as antimicrobial and antioxidant agents.[17,18] In connection with our interest in the design and production of MCRs,[19] the catalytic activity of the new Pd (II) complex towards dihydrotetrazolo[1,5-*a*]pyrimidine-6-carboxylic ester **5a**–**o** derivative synthesis using ultrasonic irradiation under mild reaction conditions should be mentioned herein.

Consequently, Cu (II), Pd (II), and Fe (III) complexes were synthesized and structurally elucidated by all available techniques. After that, the catalytic protocol was conducted through four-component coupling reactions. Cyanoguanidine, sodium azide, aromatic aldehydes, and *ß*-ketoesters were the components used for synthesis by ultrasonic irradiation in green solvent, to produce aimed bio-active heterocyclic compounds. The target products have been deposited in excellent yields through facile reaction. The catalytic behavior has been supported through crystal packing properties as well as DFT-quantum parameters.

2 | EXPERIMENTAL

All materials and solvents were utilized as received from Sigma Aldrich or Alfa Aesar. Each device was characterized, and the measurement details were also reported in the supporting information. In addition, other essential conditions will be displayed in discussion part, separately.

2.1 | Instrumentation and methods

All physical measurements and requirements of each system used in this study were reported in the supporting information. Some specifications were individually carried out in discussion portion.

2.2 | Synthesis of ARPT ligand

The ligand is prepared according to the procedures mention in a previous study[20] as follows: in a round-bottom flask (100 ml), 10 mmol of arylidenemalononitrile, 10 mmol of 2,4-thiazolidinedione, 30 mmol of EtOH, and 20 mmol of piperidine were mixed. Then the mixture was refluxed under stirring for 2 h, and arylidenemalononitrile was isolated and processed. The solid product was washed by hot EtOH and filtered off, and then the purity was checked by TLC.

2-Amino-6-oxo-3-(piperidinylamidino)-4-phenyl-6,7-dihydro-pyrano[2,3-*d*]-5,7-thiazol was the product (abbreviation; ARPT); color: pale yellow molecular formula $C_{18}H_{20}N_4O_2S$(356), mp: 235°C. *Anal*. Calcd (%): C, 60.69, H, 5.62, N, 15.77; found (%): C, 60.67, H, 5.62, N, 15.73. Solubility: ethanol.

IR (KBr pellet, cm^{-1}, Figure S1): 3398 ν(N—H), 3308–3193 $\nu(NH_2)$, 1589 ν(C═O). NMR δ in DMSO-d_6: 9.87, 7.40–7.30, 6.99, 4.64, 4.46, 3.34–3.32, and 1.55–1.46 ppm for (s, 1H, NH), (m, 5H, ArH), (s, 2H, NH_2), (d, 1H, CH), (d, 1H, NH), (t, 4H, $2CH_2$), and (m, 6H, $3CH_2$), respectively. ^{13}C NMR δ in DMSO-d_6: 24.18, 25.85, 45.68, 51.93 (alp-C), 56.19, 71.48, 118.64, 127.84, 128.12, 129.84, 142.71 (N—C—O, thiazol), 152.49 (N—C—O, pyran), 162.17 (N—C═NH), and 171.07 (C═O) (Figures 1, S2, and S3).

2.3 | Synthesis of metal complexes

Equi-molar reactants from ARPT ligand (5 mmol) and each metal salt (5 mmol), Cu (II), Fe (III) ions (in 20 ml

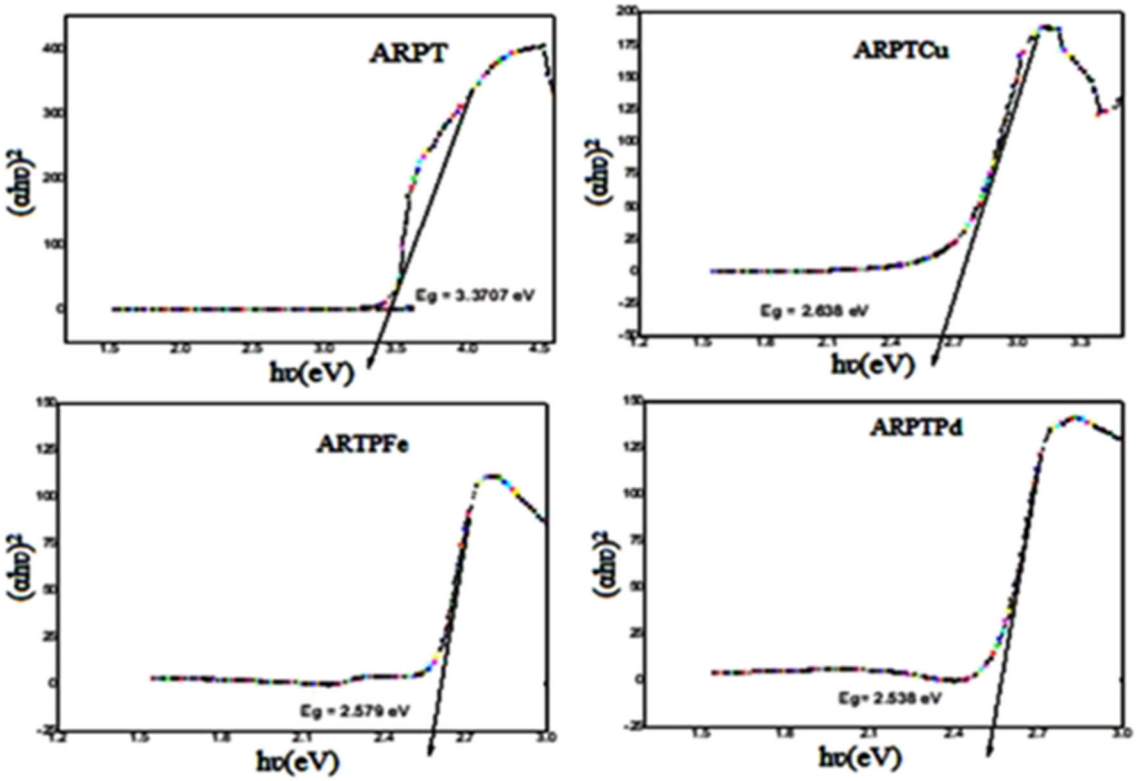

FIGURE 1 Calculated optical band gap for the tested complexes

EtOH) and Pd (II) salt (in 20 ml hot AcOH), were mixed. The mixed solutions were stirred under reflux for 2–3 h, and then the precipitates were separated and washed by hot EtOH or Aceton (Scheme 1).

[ARPTCu] (Pale green); [Cu $(OAc)_2(ARPT)(H_2O)_2$]. H_2O: Molecular formula $C_{22}H_{32}N_4O_9SCu$ (591.5), decom.t: 244°C. *Anal.* Calcd (%): C, 44.55, H, 5.52, N, 9.46, found (%): C, 44.63, H, 5.41, N, 9.46, solubility: DMF, Λm: 10.49 (Ω^{-1} cm^2 mol^{-1}), IR (KBr pellet, cm^{-1}): 3405 ν(N—H), 3314–3199 $\nu(NH_2)$, 1587 ν(C═O), 450 (M—N) and 571 (M—O).

[ARPTFe] (Brown); [Fe $(NO_3)_3(ARPT)(H_2O)$].1.5H_2O: Molecular formula $C_{18}H_{25}N_7O_{13.5}$ SFe (643.34), decom.t: 270°C. *Anal.* Calcd (%): C, 33.19, H, 3.87, N, 15.05, found (%): C, 33.18, H, 3.84, N, 15.05, solubility: DMF, Λm: 15.38 (Ω^{-1} cm^2 mol^{-1}), IR (KBr pellet, cm^{-1}): 3409 ν(N—H), 3318–3200 $\nu(NH_2)$, 1584 ν(C═O), 458 (M—N) and 533 (M—O)

[ARPTPd] (Orange); [Pd $(OAc)_2(ARPT)$].3H_2O; molecular formula $C_{22}H_{32}N_4O_9SPd$ (634.4), decom.t: 290°C. *Anal.* Calcd (%): C, 41.69, H, 5.02, N, 8.85, found (%): C, 41.61, H, 5.04, N, 8.82, solubility: DMF, Λm: 8.78 (Ω^{-1} cm^2 mol^{-1}), IR (KBr pellet, cm^{-1}): 3426 ν(N—H), 3029–3060 $\nu(NH_2)$, 1588 ν(C═O), 445(M—N) and 552 (M—O).

2.4 | Stoichiometry and formation constants of complexes in solution

Stoichiometric ratio and stability of complexes in solution were estimated according to Job's method (mole ratio and continuous variation).[20,21] The absorbance was noted for all prepared solutions after mixing (M and L) and let to equilibrate. Then schemed versus ([L]/[L] + [M]) or ([L]/[M]) (Figures S4 and S5). The formation constants (K_f) of complexes were often achieved through the spectrophotometric procedure by the following relation[22]; $K_f = A\,A_m/(1-A/A)^2$, where [A] is the absorbance values along each side of absorption peaks which randomly assigned, [A_m] is the highest absorbance for absorbance peak, and [C] is the molar concentration of the metal. In addition, ΔG^* values (free energy changes) were estimated from the following equation [$\Delta G = -RT\ \mathrm{Ln}\ K_f$] (at 25°C), where, K_f, R, and T are the constant of formation, constant of gas, and the temperature in Kelvin, respectively.

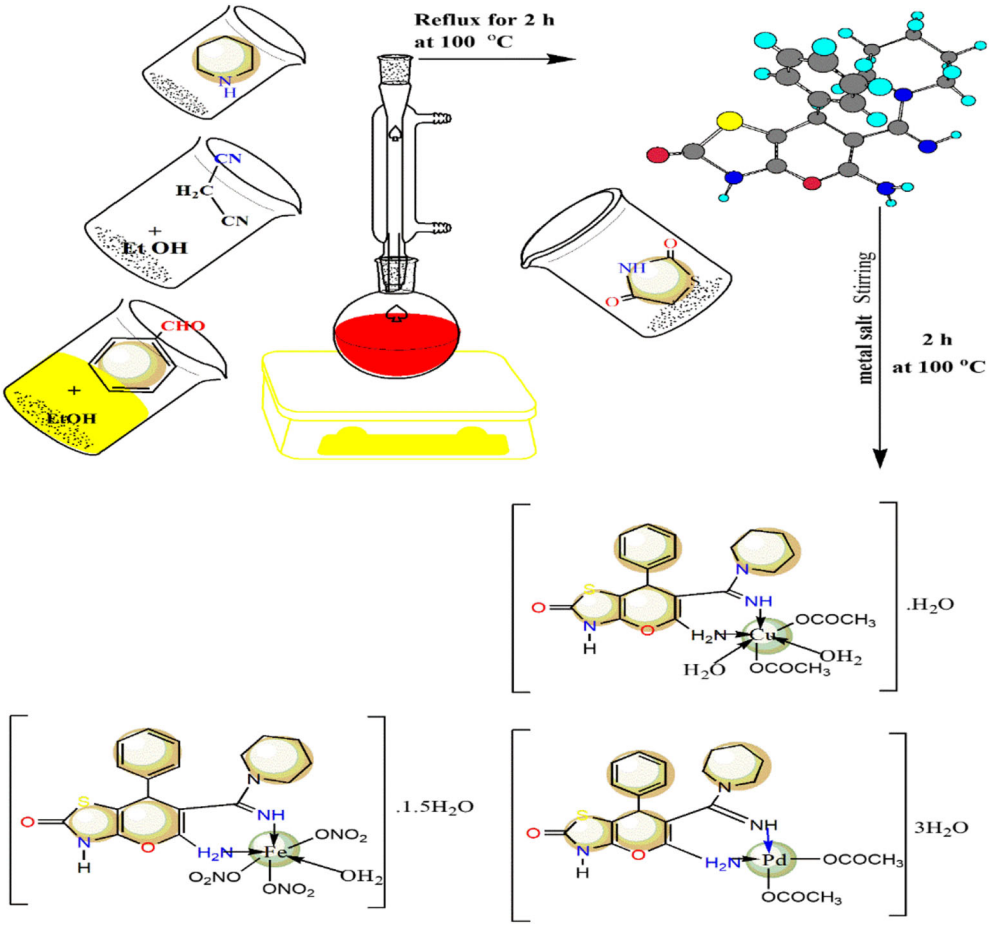

SCHEME 1 Synthetic strategy for preparation of the ligand and its complexes

2.5 | Procedure for thermo-kinetic features

Thermo-kinetic parameters were calculated regarding TGA curves for the tested complexes. Pre-exponential factor (A) and activation energy (E*), in addition to ΔS, ΔH, and ΔG, were the parameters examined. The degradation steps mostly have specific borders with a defined fraction that breaks down (α) within the step for each temperature point.

Variable researchers[23–30] developed equations for such purpose and clarified their advantages. Among those, Coat-Redfern[23] and Horowitz-Metzger[30] equations have been selected to estimate such parameters.

2.6 | Catalytic application

2.6.1 | Procedure for synthesis of dihydrotetrazolo[1,5-*a*]pyrimidine derivatives 5a–o

In a flask with round bottom, 5-aminotetrazole was prepared in situ as follows: briefly, a mixture of cyanoguanidine **1** (1 mmol) and sodium azide **2** (1.1 mmol) was dissolved in 20 ml distilled water in presence of 10 mol % Pd (II) complex (ARPTPd). Then, the mixture was sonicated at 20 kHz frequency and 40 W power at 60°C, for 10 min to give 5-aminotetrazole in approximately 100% yield. After that, an aromatic aldehydes **3** (1 mmol) and methyl or ethyl acetoacetate **4** (1 mmol) were added to reaction pot.[31,32] Next, the mixture was sonicated at 20 kHz frequency and 40 W power at 60°C, for desired appropriate time.

The reaction end was detected by thin layer chromatography (TLC). Then, the reaction mixture was allowed to cool to room temperature and filtered off the catalyst (ARPTPd). The organic materials were extracted by using ethyl acetate (3 × 10 ml). So tetrazolopyrimidine derivatives **5a–o** combined organic phase, were washed with water, dried over anhydrous Na_2SO_4, and concentrated under reduced pressure. The resulting solids were isolated and recrystallized from ethanol to give pure products. These products were characterized by melting points and spectroscopy (FT-IR and NMR).

Spectral data for the synthesized compounds

Compound **5a**: mp = 202–204°C. IR (KBr) cm^{-1} = 3184, 3090, 2940, 1712, 1593, 1521; ^1H NMR (400 MHz, DMSO-

d_6) δ = 11.46 (s, 1H, NH), 8.25 (s, 2H, ArH), 7.91 (s, 1H, ArH), 7.61 (s, 1H, ArH), 7.25 (s, 1H, ArH), 6.92 (s, 1H, CH), 4.01 (q, J = 6.9 Hz, 2H, OCH_2CH_3), 2.43 (s, 3H, CH_3), 1.08 (t, J = 6.9 Hz, 3H, OCH_2CH_3). *Anal.* Calcd for $C_{14}H_{15}N_5O_2$: C, 58.94; H, 5.30; N, 24.55. Found: C, 58.91; H, 5.32; N, 24.54.

Compound **5b**: mp = 236–238°C. IR (KBr) cm^{-1} = 3244, 3180, 3104, 2966, 1707, 1653, 1554; ^{1}H NMR (400 MHz, DMSO-d_6) δ = 11.39 (s, 1H, NH), 7.55 (d, J = 7.7 Hz, 2H, ArH), 7.26 (d, J = 7.7 Hz, 2H, ArH), 6.69 (s, 1H, CH), 3.99 (q, J = 6.9 Hz, 2H, OCH_2CH_3), 2.44 (s, 3H, CH_3), 1.03 (t, J = 6.9 Hz, 3H, OCH_2CH_3). *Anal.* Calcd for $C_{14}H_{14}BrN_5O_2$: C, 46.17; H, 3.87; N, 19.23. Found: C, 46.20; H, 3.85; N, 19.21.

Compound **5c**: mp = 185–187°C. IR (KBr) cm^{-1} = 3241, 3162, 3049, 2929, 1700, 1650, 1552; ^{1}H NMR (400 MHz, DMSO-d_6) δ = 11.41 (s, 1H, NH), 7.45 (s, 1H, ArH), 7.41 (d, J = 4.7 Hz, 2H, ArH), 7.25 (t, J = 4.7 Hz, 1H, ArH), 6.70 (s, 1H, CH), 3.97 (q, J = 6.9 Hz, 2H, OCH_2CH_3), 2.46 (s, 3H, CH_3), 1.01 (t, J = 6.9 Hz, 3H, OCH_2CH_3). *Anal.* Calcd for $C_{14}H_{14}ClN_5O_2$: C, 52.59; H, 4.41; N, 21.90. Found: C, 52.60; H, 4.39; N, 21.87.

Compound **5d**: mp = 256–258°C. IR (KBr) cm^{-1} = 3233, 3169, 3060, 2954, 1706, 1655, 1574; ^{1}H NMR (400 MHz, DMSO-d_6) δ = 11.40 (s, 1H, NH), 7.667 (s, 1H, ArH), 7.46–7.50 (m, 2H, ArH), 7.01 (s, 1H, CH), 3.96 (q, J = 6.9 Hz, 2H, OCH_2CH_3), 2.44 (s, 3H, CH_3), 1.00 (t, J = 6.9 Hz, 3H, OCH_2CH_3). *Anal.* Calcd for $C_{14}H_{13}Cl_2N_5O_2$: C, 47.47; H, 3.70; N, 19.77. Found: C, 47.44; H, 3.68; N, 19.74.

Compound **5e**: mp = 208–210°C, IR (KBr) cm^{-1} = 3182, 3090, 2924, 1720, 1654, 1578, 1534; ^{1}H NMR (400 MHz, DMSO-d_6) δ = 11.41 (s, 1H, NH), 8.24 (s, 2H, ArH), 7.78 (s, 1H, ArH), 7.67 (s, 1H, ArH), 6.94 (s, 1H, CH), 3.98 (q, J = 6.9 Hz, 2H, OCH_2CH_3), 2.48 (s, 3H, CH_3), 0.99 (t, J = 6.9 Hz, 3H, OCH_2CH_3). *Anal.* Calcd for $C_{14}H_{14}N_6O_4$: C, 50.91; H, 4.27; N, 25.44. Found: C, 50.89; H, 4.380; N, 25.41.

Compound **5f**: mp = 211–213°C, IR (KBr) cm^{-1} = 3238, 3174, 3051, 2982, 1703, 1657, 1570, 1523; ^{1}H NMR (400 MHz, DMSO-d_6) δ = 11.31 (s, 1H, NH), 6.91–6.96 (m, 2H, ArH), 6.75–6.79 (m, 1H, ArH), 6.71 (s, 1H, CH), 3.99 (q, J = 6.9 Hz, 2H, OCH_2CH_3), 3.79 (s, 6H, 2 OCH_3), 2.43 (s, 3H, CH_3), 1.02 (t, J = 6.9 Hz, 3H, OCH_2CH_3). *Anal.* Calcd for $C_{16}H_{19}N_5O_4$: C, 55.64; H, 5.55; N, 20.28. Found: C, 55.62; H, 5.57; N, 20.25.

Compound **5g**: mp = 185–187°C, IR (KBr) cm^{-1} = 3277, 3044, 2979, 1705, 1600, 1541; ^{1}H NMR (400 MHz, DMSO-d_6) δ = 11.22 (s, 1H, NH), 7.00–7.23 (m, 4H, ArH), 6.68 (s, 1H, CH), 4.01 (q, J = 6.9 Hz, 2H, OCH_2CH_3), 2.44 (s, 3H, CH_3), 1.10 (t, J = 6.9 Hz, 3H, OCH_2CH_3), 1.03 (m, 6H, $[CH_3]_2N$). *Anal.* Calcd for $C_{16}H_{20}N_6O_2$: C 58.52; H 6.14; N 25.59. Found, %: C 58.55; H 6.18; N 25.55.

Compound **5h**: mp = 188–190°C, IR (KBr) cm^{-1} = 3162, 3102, 2920, 1692, 1623, 1504; ^{1}H NMR (400 MHz, DMSO-d_6) δ = 11.44 (s, 1H, NH), 8.16 (d, J = 7.9 Hz, 2H, ArH), 7.85 (d, J = 7.9 Hz, 2H, ArH), 7.04 (s, 1H, CH), 6.87 (s, 1H, CH), 3.60 (s, 3H, CH_3), 2.40 (s, 3H, CH_3). *Anal.* Calcd for $C_{13}H_{13}N_5O_2$: C, 57.56; H, 4.83; N, 25.82. Found: C, 57.58; H, 4.86; N, 25.80.

Compound **5i**: mp = 220–222°C, IR (KBr) cm^{-1} = 3256, 3043, 2941, 1704, 1640, 1554; ^{1}H NMR (400 MHz, DMSO-d_6) δ = 11.33 (s, 1H, NH), 7.56 (d, J = 7.9 Hz, 2H, ArH), 7.28 (d, J = 7.9 Hz, 2H, ArH), 6.71 (s, 1H, CH), 3.55 (s, 3H, CH_3), 2.45 (s, 3H, CH_3). *Anal.* Calcd for $C_{13}H_{12}BrN_5O_2$: C, 44.59; H, 3.45; N, 20.00. Found: C, 44.61; H, 3.46; N, 19.98.

Compound **5j**: mp = 183–185°C, IR (KBr) cm^{-1} = 3272, 3187, 3058, 2956, 1672, 1579; ^{1}H NMR (400 MHz, DMSO-d_6) δ = 11.29 (s, 1H, NH), 7.27–7.42 (m, 4H, ArH), 6.70 (s, 1H, CH), 3.56 (s, 3H, CH_3), 2.45 (s, 3H, CH_3). *Anal.* Calcd for $C_{13}H_{12}ClN_5O_2$: C, 51.07; H, 3.96; N, 22.91. Found: C, 51.10; H, 3.98; N, 22.89.

Compound **5k**: mp = 253–255°C, IR (KBr) cm^{-1} = 3167, 3043, 2951, 1711, 1690, 1552; ^{1}H NMR (400 MHz, DMSO-d_6) δ = 11.42 (s, 1H, NH), 7.69 (s, 1H, ArH), 7.45 (s, 2H, ArH), 7.01 (s, 1H, CH), 3.54 (s, 3H, CH_3), 2.47 (s, 3H, CH_3). *Anal.* Calcd for $C_{13}H_{11}Cl_2N_5O_2$: C, 45.90; H, 3.26; N, 20.59. Found: C, 45.88; H, 3.27; N, 20.56.

Compound **5l**: mp = 225–227°C, IR (KBr) cm^{-1} = 3243, 3168, 3044, 2952, 1712, 1687, 1556; ^{1}H NMR (400 MHz, DMSO-d_6) δ = 11.42 (s, 1H, NH), 7.72–8.18 (m, 4H, ArH), 6.92 (s, 1H, CH), 3.54 (s, 3H, CH_3), 2.46 (s, 3H, CH_3). *Anal.* Calcd for $C_{13}H_{12}N_6O_4$: C, 49.37; H, 3.82; N, 26.57. Found: C, 49.33; H, 3.80; N, 26.54.

Compound **5m**: mp = 231–233°C, IR (KBr) cm^{-1} = 3187, 3053, 2937, 1699, 1554; ^{1}H NMR (400 MHz, DMSO-d_6) δ = 11.40 (s, 1H, NH). 8.21 (d, J = 7.9 Hz, 2H, ArH), 7.66 (d, J = 7.9 Hz, 2H, ArH), 6.88 (s, 1H, CH), 3.53 (s, 3H, CH_3), 2.46 (s, 3H, CH_3). *Anal.* Calcd for $C_{13}H_{12}N_6O_4$: C, 49.37; H, 3.82; N, 26.57. Found: C, 49.40; H, 3.85; N, 26.55.

Compound **5n**: mp = 219–221°C, IR (KBr) cm^{-1} = 3177, 3043, 2954, 1701, 1661, 1559; ^{1}H NMR (400 MHz, DMSO-d_6) δ = 11.31 (s, 1H, NH), 6.75–6.99 (m, 3H, ArH), 6.22 (s, 1H, CH), 3.75 (s, 3H, CH_3O), 3.71 (s, 3H, CH_3O), 3.55 (s, 3H, CH_3), 2.44 (s, 3H, CH_3). *Anal.* Calcd for $C_{15}H_{17}N_5O_4$: C, 54.38; H, 5.17; N, 21.14. Found: C, 54.41; H, 5.18; N, 21.12.

Compound **5o**: mp = 233–235°C, IR (KBr) cm^{-1} = 3371, 3035, 2944, 1691, 1568; ^{1}H NMR (400 MHz, DMSO-d_6) δ = 11.22 s (1H, NH), 6.82–7.11 (m, 4H, ArH), 6.58 (s, 1H, CH), 3.63 (s, 3H, CH_3), 2.82 (s, 6H, N $[CH_3]_2$), 2.43 (s, 3H, CH_3). *Anal.* Calcd for $C_{15}H_{18}N_6O_2$: C, 57.31; H, 5.77; N, 26.74. Found, %: C, 57.35; H, 5.79; N, 26.71.

2.6.2 | Catalyst recovery and reuse

Heterogeneous catalyst could be separated and reused easily many times, and the efficiency can be tested. The filtered catalyst was washed by ethanol and double distilled with water. After drying at 90°C for 3 h, the catalyst was recycled for another reaction-run under the same conditions.

2.7 | Geometry optimization

Materials Studio package[33] was used to simulate and optimize the studied compounds. This software was developed by Accelrys, to configure the structural forms and obtain essential quantum data. This was executed by DMOL3 program under DFT/B3LYP method through double numerical plus polarization basis set (DNP), which recommended for transition metal ion complexes.[34] The program already proceeded without any constrain under Becke3–Lee–Yang–Parr (B3LYP) of exchange-correlation functional within GGA and RPBE functionals.[35] The frequency values (positive) are the major determiner for suitability of structural forms obtained. Time-dependent DFT (TD-DFT) was applied through polarizable continuum model. Moreover, integral equation formalism variant (IEF-PCM) was used through B3LYP level to evaluate characteristics of ground or excited state.[36]

3 | RESULTS AND DISCUSSION

3.1 | General properties

The tested complexes were instituted to require ligand: metal ratio to be 1 ARPT: 1 Metal. According to physical and analytical data of ARPT ligand and its complexes, there was a good agreement between CHN microanalyses and the chemical formulae suggested. The conductivity measurements performed in DMF and proved that the complexes are non-electrolytic due to low molar conductivity values, as represented above.[37,38]

3.2 | IR and ^{1}H NMR spectroscopy

The sharp bands at 3398 and 3193–3308 cm^{-1} were assigned to ν(NH) and $\nu(NH_2)$ in ARPT ligand. But these bands were moved sequentially (at ~3405, 3409, and 3426 cm^{-1}) and (at ~3199–3314, 3200–3318, and 3029–3060 cm^{-1} ranges) in ARPTCu, ARPTFe, and ARPTPd complexes. This appearance indicates the coordination of (NH) and (NH_2) groups. A sharp band at 1589 cm^{-1}, which was assigned to ν(C═O) in the ARPT ligand, was slightly shifted to ~1587, 1584, and 1588 cm^{-1} in the metal chelates, which reflects its absence from coordination.[39]

Additionally, the bands at the lower wavenumber region are assigned to ν(M—O) and ν(M—N) vibrations (Figure S1, i. e.). Other significant bands appeared at 1495 and 1384 cm^{-1} in ARPTCu spectrum and at 1430 and 1375 cm^{-1} in the ARPTPd spectrum, which coincide with υ_{as} (OAc) and υ_s (OAc) vibrational, respectively.[40] Furthermore, bands at 1452 and 1378 cm^{-1} appeared in the ARTPFe spectrum and assigned to υ_{as} (NO_3) and υ_s (NO_3), respectively. The separation between two bands ($\Delta = \upsilon_{as}$-υ_s) is high enough to judge on monodentate nature of the conjugated anions (OAc^- and NO_3^-).

^{1}H NMR spectrum of PTP ligand (in DMSO-d_6, Figure 1) showed three singlet signals at δ (ppm); 9.87 (s, 1H, NH), 4.64 (s, 1H, CH), and 4.46 (s, 1H, NH). Also, doublet signal at δ (ppm); 6.99 (d, 2H, NH2), triplet signal at δ (ppm); 3.34–3.32 (t, 4H, 2CH2) ppm, multiplet signals at δ (ppm); 7.40–7.30 (m, 5H, ArH) and 1.55–1.46(m, 6H, 3CH2) range, appeared. ^{13}C NMR spectrum of PTP ligand (Figure 2) presented a sharp signal at 171.07 ppm due to C═O. Also, sharp signals at 162.17, 56.19–152.49, and 24.18–40.83 ppm due to N—C═NH, 8CH—Ar, and 4CH2—Aliph, respectively. ^{1}H NMR spectral data in ARTP ligand exhibit the following remarks: signals at δ (ppm); 9.87 (s, 1H, NH), 7.40–7.30 (m, 5H, ArH), 6.99 (d, 2H, NH2), 4.64 (d, 1H, CH), 4.46 (d, 1H, NH), 3.34–3.32 (t, 4H, 2CH2), and 1.55–1.46 (m, 6H, 3CH2) range.[20] ^{13}C NMR spectrum of the ligand displayed band at 190.96 ppm for C═O, band is appreciated at 162.42 ppm for N—C═NH, about 56.03–152.5 ppm for 4CH—Ar seemed and 24.19–51.22 ppm for $4CH_2$—Aliph[41] (Figure S2 and S3).

3.3 | Electronic spectroscopy

Electronic transitions within the ligand and its complexes happened under influence of UV–Vis light as intraligand, charge transfer (CT), and ligand field splitting. This scanning was executed in DMF (at RT) over 200–800 nm range (Figure S6). Functional transitions were extracted and assigned (Table S1) to examine changes in the bands due to complexation. Ligand spectrum exhibited absorption band belongs to $n \rightarrow \pi^*$ transition. Regarding ARPTCu complex spectrum, different bands belong to $\pi \rightarrow \pi^*$, $n \rightarrow \pi^*$, and CT appeared beside the band at 410 nm, which assigned to $^2Eg \rightarrow {}^2T_2g$ transition in octahedral form. Regarding ARPTFe complex spectrum, bands of intraligand transitions and CT appeared in

FIGURE 2 Recyclability of ARPTPd in the model reaction

addition to a band at 532 nm which assigned to $^6A_{1g} \rightarrow {}^4T_{2g}$ transition within high spin octahedral form. Regarding ARPTPd complex spectrum, bands of $n \rightarrow \pi^*$, $\pi \rightarrow \pi^*$, and CT transitions, appeared in addition to a band at 450 nm, which assigned to $^1A_{1g} \rightarrow {}^1A_{2g}$ transition in square-planer form.[20,42,43]

According to UV–Vis spectra, energy separation between the ground and excited states (optical band difference, E_g) can be measured. An important indicator of distinct properties such as conductivity, optical properties, and catalytic activity is the distance between the valence band and the conduction band. The minimum quantum ($h\upsilon$) essential to expel electron from its ground state to another exited level and leaving a positive hole although the attraction force in between is known by the optical band gap energy (E_g). The lower the gap value, the closeness valence band and conduction band, which facilitates excitation and leading to optical or conductivity property.[44] This gap is known theoretically as the separation between HOMO and LUMO levels, which points to activation energy value and semiconductors-like property.[44] As known, the optical band gap energy value of Si as a standard semiconductor is 1.14 eV, which is sufficiently lower to a significant level of conducting feature. The calculated values for ARPTPd, ARPTFe, and ARPTCu complexes are 2.538, 2.5.79, and 2.638 eV, respectively (Figure 4). The lower value of the ARPTPd complex predicts its distinguish optical property as well as the lower activation energy needed for any application as a catalytic role in any heterogamous catalysis. Optical band gap value can be obtained by a facilitated method as follows:

$$\alpha = 1/d \ln A \quad (1)$$

where d is the cell width.

$$\alpha h\upsilon = A\left(h\upsilon\text{-}E_g\right)^m \quad (2)$$

where α and A are the absorption coefficient and energy independent constant.The value of m differentiates direct or indirect transition at m = 0.5 or 2, respectively. So, calculating α values from Equation 1 to be used in Equation 2 and then calculates $(\alpha h\upsilon)^2$ values. Draw graphical relation between $(\alpha h\upsilon)^2$ and $h\upsilon$ (Figure 1) and extrapolating a straight line to interact with *x*-axis at $(\alpha h\upsilon)^2 = 0$, the E_g value could being obtained.[34]

3.4 | TGA and kinetic aspects

TGA was executed for ARPT complexes up to 25–800°C range, to examine their thermal stability and put a suitable degradation scheme along the decomposition stages appeared. The curves obtained for the complexes appeared relatively identical that reflects the same degradation pathways (Scheme S1). All complexes reveal lower thermal stability due to the presence of crystal water is expelled below 120°C. Four degradation steps were recorded till 700°C in all TGA curves, and the residual parts coincide with stable metal oxide. The suggested mass-decompose was tabulated (Table 1), and the high conformity between the calculated and found percentages reflects the exact determination for step borders without overlapping between follower steps.[20,45,46]

Moreover, to illustrate the characteristics of degradation phases, kinetic, and thermodynamic parameters were determined for degradation phases.[47]

1- After removing crystal water molecules in the first step, higher activation energy values recorded particularly with ARPTPd and ARPTFe complexes mean the greater the stability of them.
2- The negative ΔS sign refers to ordered activated complex, and the degradation process has non-spontaneous nature.

TABLE 1 Plausible degradation attributes as well as thermo-kinetic parameters

Complexes	Temperature (°C)	Fragment loss %		Weight loss %		E^* (kJ mol^{-1})	A (S^{-1})	ΔH^* (kJ mol^{-1})	ΔG^* (kJ mol^{-1})	ΔS^* (Jmol^{-1} K^{-1})
		Molecular formula	Mol. Wt.	Found	Calcd					
ARPTCu	36–120°C	H_2O	18	3.08	(3.04)	43.79	0.58	56.17	76.68	−262.901
	122–350°C	$C_4H_{10}O_6$	154	26.01	(26.03)			54.86	119.078	−272.108
	352–550°C	$C_{12}H_{16}N_2$	188	31.76	(31.78)			53.07	178.22	−277.493
	552–700°C	$C_6H_4N_2SO$	152.07	25.67	(25.70)			51.618	227.036	−280.22
Residue	>700°C	CuO	79.55	13.43	(13.44)					
ARPTFe	36–125°C	$1.5H_2O$	27	4.25	(4.14)	70.89	0.25	70.22	91.09	−260.845
	127–350°C	$(NO_3)_3 + H_2O$	204	31.2	(31.29)			68.91	133.15	−269.911
	352–485°C	$C_{11}H_{16}N_2$	188	28.88	(28.84)			67.41	182.19	−274.595
	490–700°C	$C_6H_4N_2SO$	152.07	23.30	(23.33)			65.94	231.07	−277.531
Residue	>700°C	$0.5Fe_2O_3$	79.8	12.15	(12.24)					
ARPTPd	35–110°C	$3H_2O$	54	8.48	(8.51)	93.93	0.35	93.34	111.78	−256.204
	115–280°C	$C_4H_6O_4$	118	18.65	(18.60)			92.30	144.42	−264.574
	282–400°C	$C_{12}H_{16}N_2$	188	29.7	(29.63)			91.10	182.8	−269.136
	405–700°C	$C_6H_4N_2SO$	152.07	23.90	(23.97)			89.35	240.12	−273.141
Residue	>700°C	PdO	122.4	19.25	(19.29)					

3- The positive sign of ΔH implies endothermic conditions of degradation stages.
4- The positive sign of ΔG indicates nonspontaneous decomposition behavior, and TΔS values increased from step to another and led to increase ΔG values.

3.5 | Studies in solution

3.5.1 | Stoichiometry and formation constant of complexes

Molar ratio and continuous variation routes were applied to evaluate stoichiometry of tested complexes through their formation in solution by reaction of ARPT ligand and each metal ion [Fe (III), Pd (II), and Cu (II)]. As displayed (Figures S4 and S5), the highest absorbance in the curve was detected at mole fraction (X = 0.5) according to 1 metal: 1 ligand ratio. Using a continuous variation process, spectrophotometric measurements were used to calculate formation constants (K_f) of complexes. High K_f values appeared with all tested complexes, which reveal stability in the following order of ARPTFe > ARPTCu > ARPTPd. Due to negative Gibbs free energy, the reaction between metals and ARPT ligand was desirable and spontaneous.[48]

3.5.2 | Influence of pH variations

The curves obtained for three complexes under variable pH values (Figure S7) appeared identical, and the steady range was broad enough along pH = 4–10 range. This wide range facilitates their applications at different basicity levels without affections.[20,49]

3.6 | Catalytic role of ARPTPd complex by ultrasonic irradiation

3.6.1 | Synthesis of dihydrotetrazolo[1,5-*a*] pyrimidine derivatives **5a–o**

The catalytic activity of palladium (II) complex (ARPTPd) seems to be a promising eco-friendly catalyst in facile one-pot synthesis for hybrid molecules dihydrotetrazolo[1,5-*a*]pyrimidine-6-carboxylic esters **5a–o** using ultrasonic irradiation. This was done through coupling reaction between four components as cyanoguanidine **1** (1 mmol), sodium azide **2** (1.1 mmol), aromatic aldehydes **3** (1 mmol), and methyl or ethyl acetoacetate **4a**,**b** (1 mmol), in water using ultrasonic irradiation under mild conditions.

In studied experiments, the condensation reaction was monitored under influence of significant factors as, catalyst dose, ultrasonic irradiation, solvent used, different Lewis acid and basic or ionic liquid catalysts on the catalytic activity. The condensation reaction performed without the catalyst and ultrasonic irradiation consumed a long reaction time. When used ultrasonic irradiation only without catalyst, the product got more yield at a longer reaction time. Although both suggested catalyst (ARPTPd) and ultrasonic irradiation, the yield of products and reaction time was improved (Scheme 2). A series of aromatic aldehydes **3** that undergo electrophilic substitution reactions are successfully synthesized in excellent yields as displayed in Scheme 2.

3.6.2 | Effect of catalyst loading

The effect of catalyst amounts on product yields was studied, and the data were presented (Table 2). In particular, loading of catalyst from 3 to 10 mol % improved the product yield from 13% to 98%. Increasing the product yield with increasing ARPTPd amount may refer to an increase in the number of available active sites and an increase in collision chance between catalyst surface and reactants molecules. Notably, the further increase in catalyst amount from 10 to 11 mol %, and the yields and reaction times did not change significantly. Therefore, 10 mol % of catalyst was the optimal amount used.

3.6.3 | Effect of solvents

Based on attempts to reach the best conditions, we must choose the effective solvent among several classical solvents, till reach the best one (Table 3). The role of solvent was investigated with reaction **5a** (i. e.). The outcomes (Table 3) suggested better effect of polar protic solvents (MeOH, EtOH, AcOH, and H_2O), which exceed the aprotic solvents (DCM, DMF, THF, CH_3CN, and $CHCl_3$). This may be due to extent of solubility for reactants in polar solvents without coordination probability with the complex. Also, it is evident that water solvent is the best choice for targeted condensation reaction, which is a preferable green synthesis approach.

3.6.4 | Effect of various Lewis acid, basic or ionic liquid catalysts

Recently, Pd (II) complexes had a lot of attention as mild Lewis acid, basic or ionic liquid catalysts for many

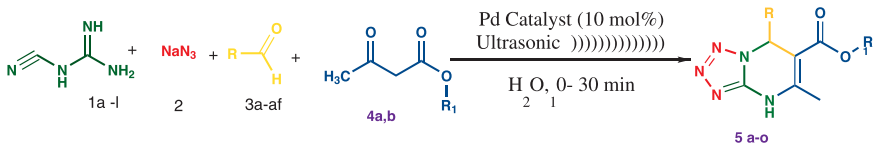

SCHEME 2 Dihydrotetrazolo[1,5-*a*] pyrimidine derivatives **5a–o** time of reaction (min) and yield (%)

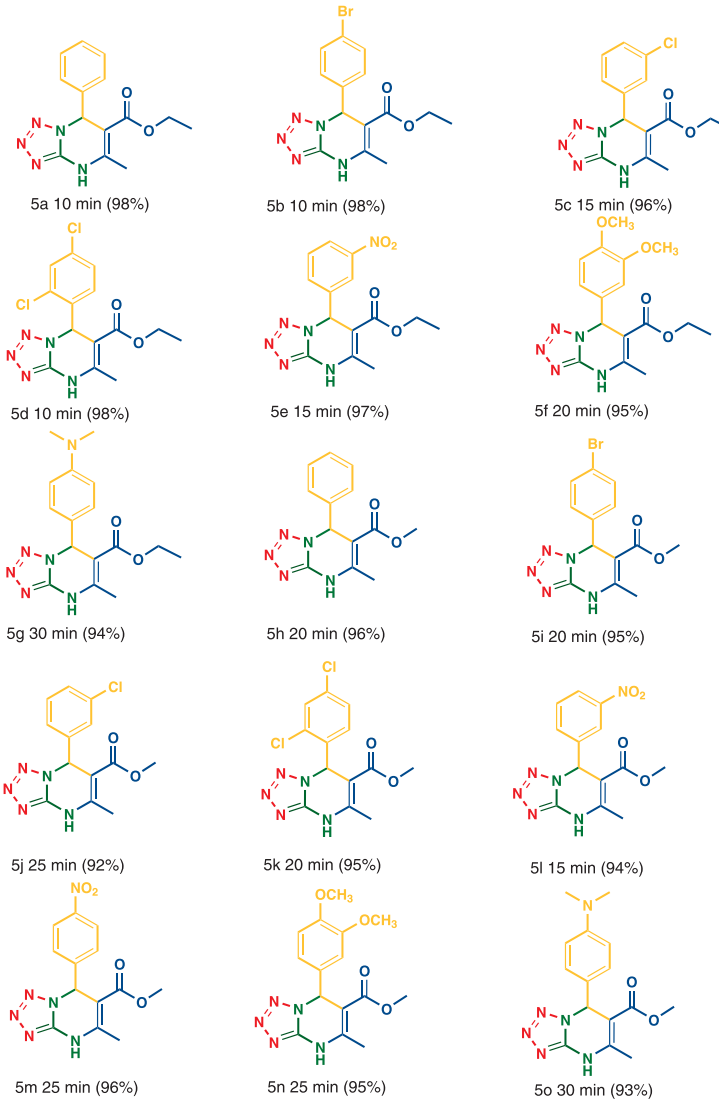

organic transformation reactions. The reaction of cyanoguanidine **1**, sodium azide **2**, aromatic aldehydes **3**, and ethyl acetoacetate **4**, at the same conditions but without catalyst and ultrasonic irradiation, a trace of the product was the only obtained (Table 4, entry 1). When we have used ultrasonic irradiation, only the product was got more yield at a longer reaction time (Table 4, entry 2). We have tested variable Lewis acids, basic catalysts, or ionic liquid to differentiate their effectiveness. By using Brønsted or Lewis acids catalysts such as $AlCl_3$, Pd $(OAc)_2$, $FeCl_3.6H_2O$, $ZnBr_2$, $CuCl_2$, CuO, and PTSA, the product yield in each case is very low (Table 4, entries 3–9). Using the basic catalyst and ionic liquid such as Et_3N, piperidine, TBABr[c], or [EMIM]Cl[d], the product yield was slightly improved than the previous case (Table 4, entries 10–13). It is worthy to note that ARPTPd catalyst was a much better one in comparing to all others catalysts studied and yield product by 98% yield (Table 4, entry 16).

3.6.5 | Recycling of catalyst

The effectiveness of this heterocyclic strategy was measured by the magnitude of recovery for the solid catalyst to be used in following cycles, as an economic feature. Consequently, the planned model reaction (cyanoguanidine **1**, sodium azide **2**, aromatic aldehydes

TABLE 2 Amount of catalyst used for synthesis of dihydrotetrazolo[1,5-*a*] pyrimidine derivatives **5a**[a]

Entry	Cat. mol%	Yield %[b]	Entry	Cat. mol%	Yield %[b]
1	3	13	5	8	84
2	5	32	6	9	92
3	6	56	7	10	98
4	7	73	8	11	98

[a]Reaction conditions: **1** (1 mmol), **2** (1.1 mmol), benzaldehyde **3** (1 mmol), and ethyl acetoacetate **4a** (1 mmol) in water by ultrasonic irradiation condition, 10 min.
[b]Isolated yields based on **5a**.

TABLE 3 Effect of solvent on synthesis of dihydrotetrazolo [1,5-*a*]pyrimidine derivatives **5a**[a]

Solvent	Time (min)	Yield (%)[b]
DCM	60	47
DMF	60	56
THF	60	56
CH_3CN	60	61
$CHCl_3$	60	67
MeOH	30	77
ACOH	30	81
EtOH	10	92
H_2O	10	98

[a]Reaction conditions: **1** (1 mmol), **2** (1.1 mmol), benzaldehyde **3** (1 mmol), ethyl acetoacetate **4a** (1 mmol), and ARPTPd catalyst (10% mol) in water by ultrasonic irradiation condition, 10 min.
[b]Isolated yields based on **5a**.

TABLE 4 Different catalysts used for reaction **5a**

Entry	Cat (mol%)	Conditions[a]	Yield (%)[b]
1	No catalyst, No US	Water, 1 day	Trace
2	No catalyst	Water, 1 h	47
3	$AlCl_3$ (10)	Water, 10 min	39
4	$FeCl_3.6H_2O$ (10)	Water, 10 min	59
5	$ZnBr_2$(10)	Water, 10 min	62
6	$CuCl_2$(10)	Water, 10 min	63
7	CuO(10)	Water, 10 min	55
8	Pd $(OAc)_2$(10)	Water, 10 min	78
9	PTSA (10)	Water, 10 min	66
10	Et_3N (10)	Water, 10 min	71
11	Pipyridine (10)	Water, 10 min	77
12	TBABr[c] (10)	Water, 10 min	62
13	[EMIM]Cl[d] (10)	Water, 10 min	69
14	ARPTCu (10)	Water, 10 min	88
15	ARPTFe (10)	Water, 10 min	91
16	ARPTPd (10)	Water, 10 min	98
17	ARPTPd (10) No US	Water, 10 min	90

[a]Reaction conditions: **1** (1 mmol), **2** (1.1 mmol), benzaldehyde **3** (1 mmol), and ethyl acetoacetate **4a** (1 mmol) in water by ultrasonic irradiation condition, 10 min.
[b]Isolated yields based on **5a**.
[c]Tetrabutylammonium bromide.
[d]Ethyl-3-methylimidazolium chloride.

3, ethyl acetoacetate **4a**, and H_2O as a solvent, by ultrasonic irradiation, 10 min) that carried out in presence of ARPTPd was studied six times for synthesis of compound **5a**, approximately by the same efficiency (Figure 2). But when we tried other next runs (6–9) under the same conditions, gave low catalytic activity.[49]

3.6.6 | Expected mechanism for catalytic behavior in synthesis process

We proposed a plausible mechanism for the synthesis of dihydrotetrazolo[1,5-*a*]pyrimidine derivatives **5a–o** as outlined in Scheme 3. It is conceivable that 5-aminotetrazole **6** was produced in the presence of ARPTPd catalyst by ultrasonic irradiation by condensation of cyanamide (in situ created from its stable chemical equivalent 1) with sodium Azide 2. Michael acceptor α,β-unsaturated **7** was formed by Knoevenagel condensation from another parallel reaction of benzaldehyde **3** and ethyl acetoacetate **4**.[50] Then, intermediate **8** was formed from a nucleophilic Michael addition for 5-aminotetrazole **6** to **7**. Finally, it was followed by intramolecular nucleophilic addition of NH_2 group of enamine tautomer of **8** to the second keto CO group, to give compound **9**, which changed to target product **5a** after releasing H_2O molecule.

3.7 | Theoretical aspects

3.7.1 | Hirshfeld crystal packing

Using Crystal Explorer software 3.1,[51] the virtual crystal model can be demonstrated for the studied complexes

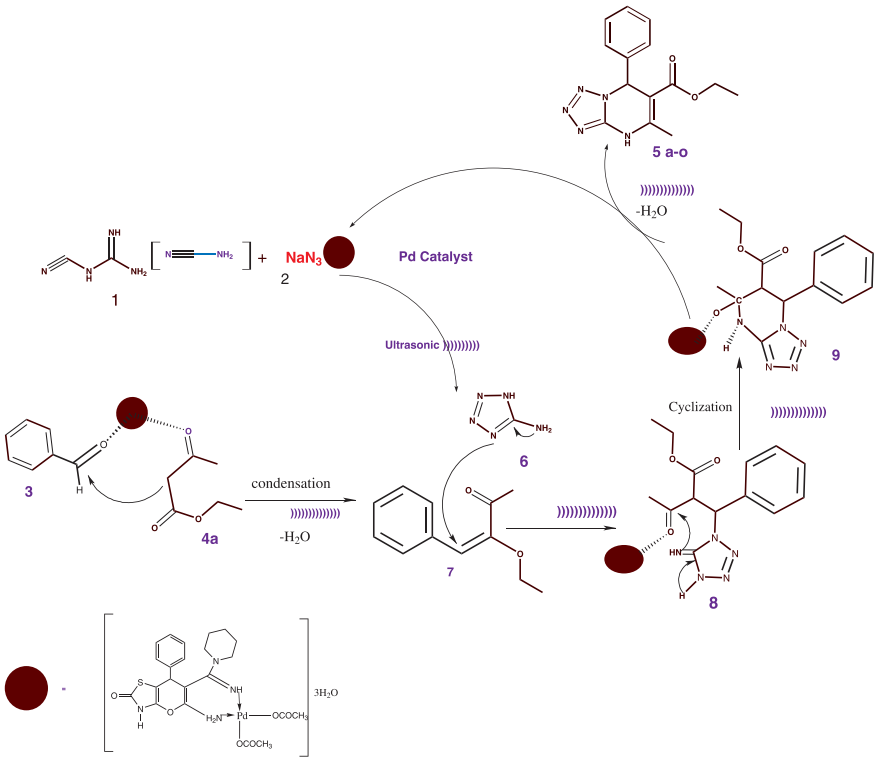

SCHEME 3 Suggested mechanism for synthesis of dihydrotetrazolo[1,5-*a*] pyrimidine derivatives and the catalytic role of ARPTPd by ultrasonic irradiation condition

after orientation steps through the VESTA package.[52] This study gives a good view about contact strength inside crystal packing, morphology, and elemental contribution in crystal contacts. All these properties conduct to evaluate the catalytic behavior of tested complexes. Three-dimensional models for the complexes were built by normalized contact distance (d_{norm}) and fragment patches (Figure 3). Normalized contact distance model (d_{norm}), divided crystal surface to zones according to contact strength with other neighboring crystals. Such zones were chromatically displayed by red, white, and blue colors that correspond to strong, moderate, and weak contact, respectively. The contact strength between neighboring surfaces was adapted based on van der Waals radii as short, moderate, or long contact-length, which categorize the contact from strong to weak. H-bonding is the interaction type between crystal surfaces. As seen (Figure 3), the red spot was appeared around the central atom particularly the secondary ligand coordinating (OAc^-, NO_3^{-2}, and H_2O), which indicates their closeness to contact, whereas the fragment patches colors are referred to the degree of proximity with other neighboring molecules. Reddish-brown spot is the closest contact zone with neighboring crystal.[52] On the other hand, 2D fingerprint plots were extracted to identify the contribution of elements in contact strength between particles (Figure S6). Accordingly, the contribution of oxygen atom in the packing systems of complexes was obviously appeared by 7.4%, 9.2%, and 16.0% with ARPTCu, ARPTPd, and ARPTFe crystals, respectively. The effective presence of oxygen atoms in the crystal surface may initiate trapping the compounds on the surface easily, which is considered the first step in any catalytic behavior inside the reaction medium.[53] ARPTPd and ARPTFe crystals have this property.

Some crystal parameters (Table 5) as volume, surface area, globularity, and asphericity were calculated, and the data suggest distinguish surface properties of ARPTPd and ARPTFe complexes. As known, morphology, surface area, and particulate shape have a significant impact in the catalytic role commonly. Also, the unit cell of each complex was built using the VESTA package and appeared by face-centered cubic (ARPTCu) or body-centered cubic shape. The unit cell obtained presented the central metal atom far from each other, which prevents their interaction.

3.7.2 | Global reactivity and MEP maps

DMOL3 program was used to ordinate the structural forms of ARPT ligand and its complexes till obtain the best geometry. The DFT method was used under Becke3–Lee–Yang–Parr (B3LYP) exchange-correlation functionals and according to DNP basis set, the structural forms were optimized (Figure S7). Ligand configuration represents suitable distribution for $N(19)H_2$ and N(18)H groups, which helps for their coordination towards the

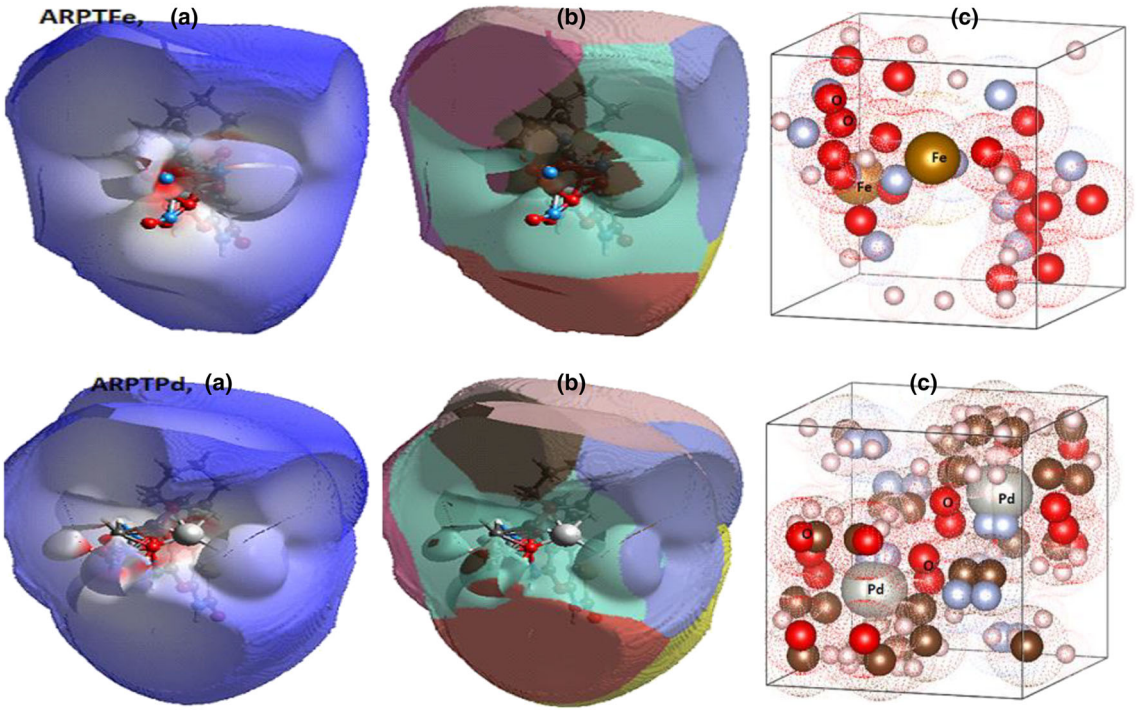

FIGURE 3 Crystal models of d norm (a), fragment patches (b), and unit cell of ARPTCu, ARPTFe, and ARPTPd complexes

TABLE 5 Hirshfeld crystal packing properties for ARPT complexes

Properties	ARPTFe	ARPTPd	ARPTCu
Volume (Å^3)	1960.28	2158.27	1872.63
Area (Å^2)	1211.09	1242.41	1187.18
Globularity	0.749	0.707	0.753
Asphericity	0.046	0.022	0.010

metal ions via neutral bidentate mode of bonding.[54] Also, the structural forms of complexes exhibited significant elongation for C(17)—N(18) and C(4)—N(19) bonds, due to coordination of nitrogen atoms, whereas the other bond lengths did not suffer any strain. Moreover, important quantum parameters were calculated to evaluate and rank stability of formed complexes according to different energy content kinds (Table S2). The energy content of complexes reflects their high stability in comparing with free ARPT ligand, whereas the lower stability recorded for ARPTPd complex, due to its four-coordination number, which reveals less stability than six-coordination that appeared with the other complexes. This less stability is preferable in cyclic reactions as catalytic process. Also, the energy gap between E_{LUMO} and E_{HOMO} levels appeared low with ARPTPd complex, which points to the ease of electronic transitions between frontier orbitals at low activation energy.[55]

Furthermore, the frontier maps (Figures 4) exhibited well distribution for the two opposing orbitals (HOMO and LUMO) on the whole molecule except piperidine and benzene zones. This perfect distribution that covered coordinating functional groups explains flexibility in electron pair donation during coordination.[56] Electrostatic potential maps (MEP) were also established over cubic contour (Figure 5) to differentiate nucleophilic and electrophilic attack zones beside the neutral one. This differentiation was done chromatically by red, blue, and green colors, respectively. Suitable nucleophilicity was noticed with N(19)H_2 and N(18)H groups, which sufficient for their interaction with positive centers as metal ions.[57]

Fukui indices were also calculated utilizing perfect conditions of DFT-semi-core pseudopods values (dspp) with polarization functional (DNP) and double numerical basis sets.[36] Under a double numerical polarization (DNP) basis set, Fukui indices for all complexes were computed using the DMol3 module. Established equations were used to calculate the global reactivity indices as softness, electrophilicity, hardness and electronegativity (Table S6).[58] The magnitude of nucleophilic (f_k^+), radical ($f_k{}^0$), and electrophilic (f_k^-) attack was estimated (Tables S3–S5). On N(18) and N(19) sites, a high nucleophilic (f_k^+) attack may occur, whereas this feature was significantly reduced after complexation due to their coordination (Table S4). ARPTPd complex exhibited the higher electrophilicity (Tables S4 and S5), which indicates its superiority in nucleophilic attack. Also, the

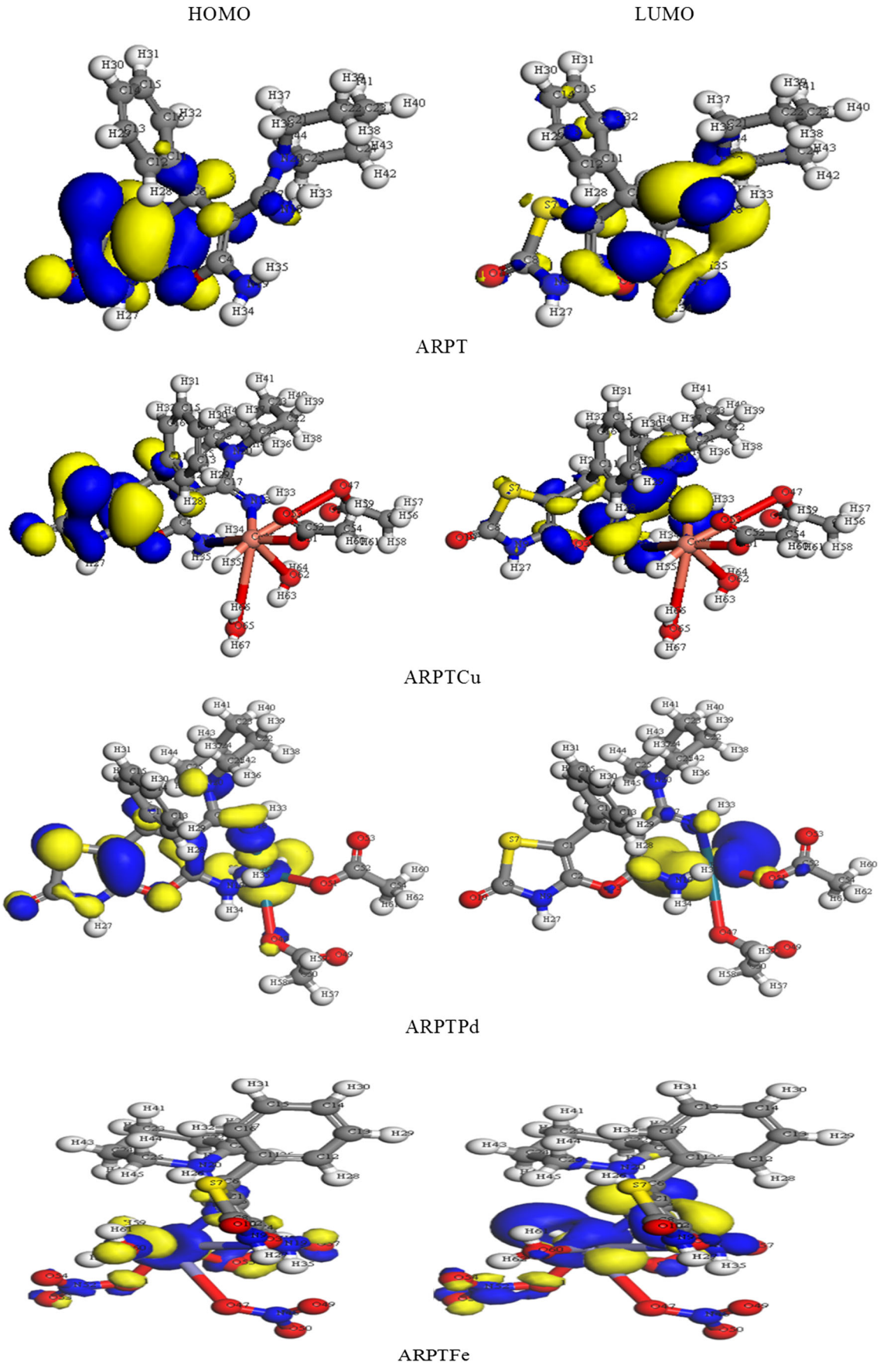

FIGURE 4 Frontiers orbitals for ARPT ligand and its complexes

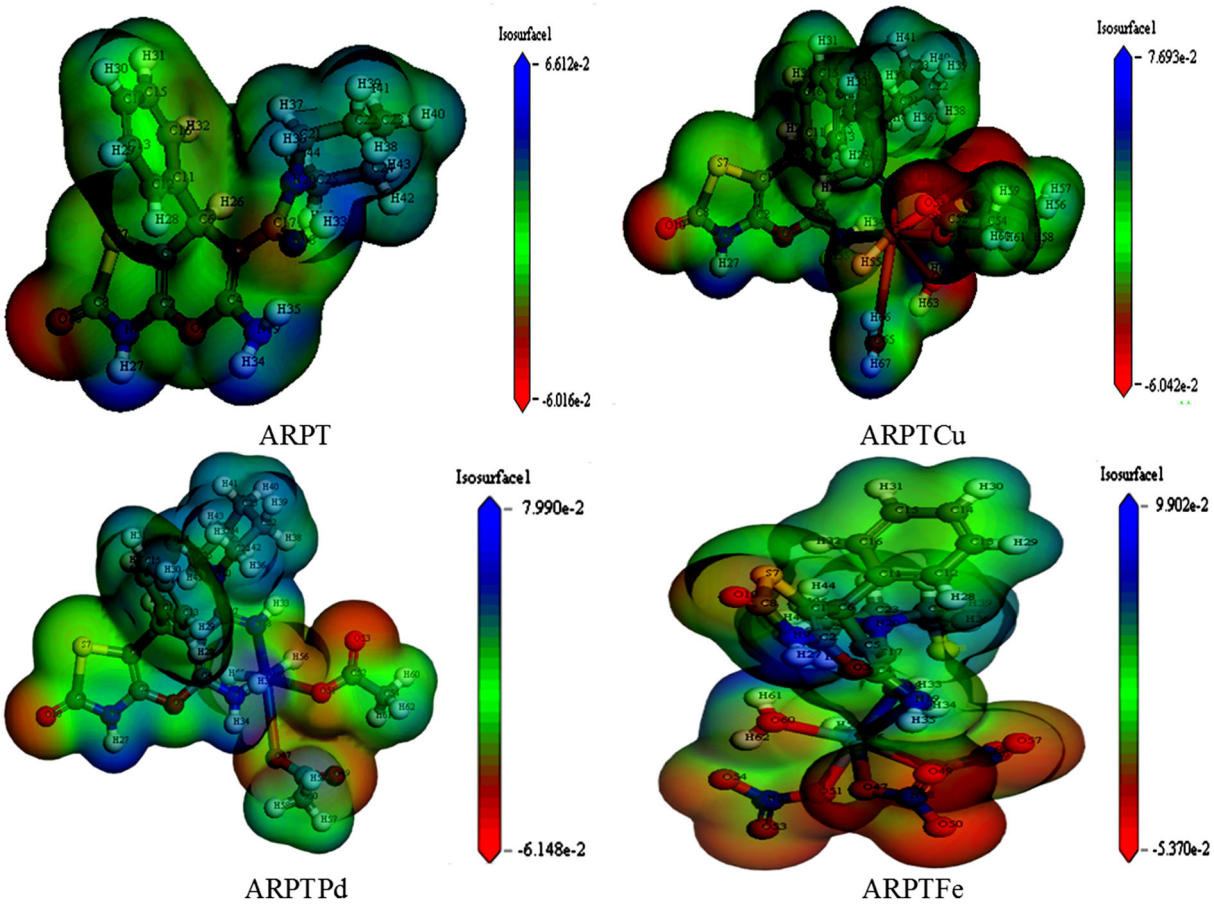

FIGURE 5 MEP maps for ARPT ligand and its complexes

overall global softness (δ) and global electrophilicity (ω) were estimated (Table S6). The softness of ARPTPd complex appeared high to significant level, which is preferred in many applications. Electrophilicity indices, on the other hand, were found to be important in ARPTFe and ARPTpd complexes, which indicate the lack of electron density over the two molecules.[58] This feature points to its ability for acquiring electrons or extra-coordinate bonds. This feature is very significant for the suggested catalyst to be success. The intermediate compounds appeared having a different coordination number than the original catalyst which mainly exceeded.

3.7.3 | Supporting information for catalytic behavior

Finally, we could summarize the promising properties of the ARPTPd complex towards catalytic uses as follows:

1- First of all, the square-planer geometry of the complex is considered the effective supporter for its distinguish catalytic behavior. This is due to the presence of two vacant sites over the *z*-axis capable of interaction till reach to five or six coordination in intermediate states without the necessity of substituting any secondary ligand.
2- Crystal properties of ARPTPd complex exhibited broad surface area of the complex which is favorable in catalysis, in general. Also, oxygen atoms have an effective contribution in contact interaction with other surfaces, oxygen could initiate trapping the compounds over the surface, which is considered the first step in any catalytic behavior inside the reaction medium.
3- Also, the energy gap (ΔE) recorded with Pd (II) complex, appeared low which points to ease of transition between two frontier orbitals under lower activation energy. Moreover, the intermediate compounds as **6**, **7**, and **9** that suggested during the synthesis process for dihydrotetrazolo[1,5-*a*]pyrimidine (Scheme 3) in presence of ARPTPd catalyst were optimized to evaluate their stability level. This optimization was carried out by using Gaussian09[59] under DFT/B3LYP method and valence double-zeta polarized basis set (6-31G*). Because orbitals of the same form must be equivalent, even if they are chemically un-equivalent in the molecule, the double zeta

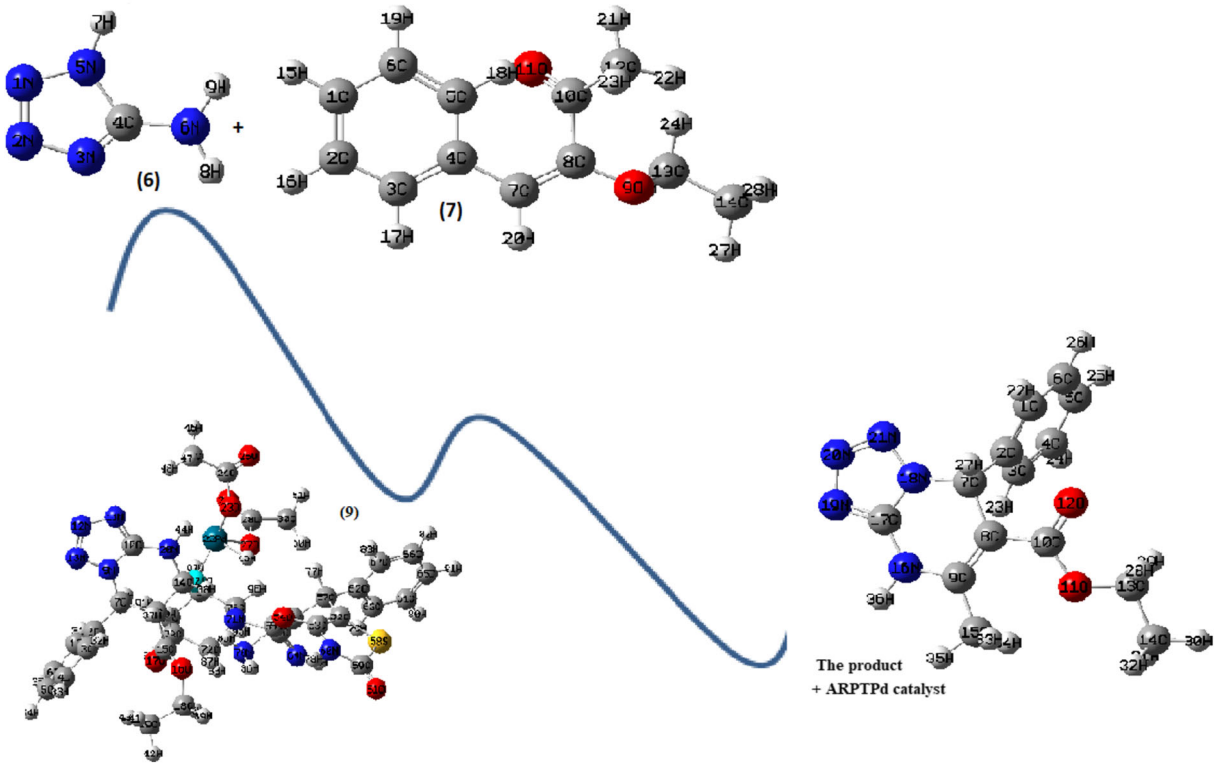

SCHEME 4 Summary of catalytic reaction stepwise to produce dihydrotetrazolo[1,5-*a*]pyrimidine

functions are needed. Compared with LANL2DZ basis set, the DFT method produces results that were significantly closer to experimental evidence. The formation energy of intermediates (**6**, **7**, and **9**), as well as the final product, was E (a. u.), −313.3612, −612.7316, −219.2425, and −961.304, respectively. This indicates the relative stability of **6** and **7**, compound **9** is highly unstable, whereas the final product is highly stable. The stability of compounds **6** and **7** predicts the proceeding of synthesis process directly. The instability of compound **9** explains the ease of isolation for the complex from compound **9** to obtain the product as well as the catalyst again (Scheme 4).

4 | CONCLUSION

A series of Cu (II), Fe (III), and Pd (II)-thiazole complexes were synthesized and characterized by analytical and spectral tools. In four- to six-coordination geometry, the ligand acted as a neutral bidentate. ARPTPd was successfully used as a catalyst in the synthesis of bioactive compounds as dihydrotetrazolo[1,5-*a*]pyrimidine derivatives from cyanoguanidine **1**, sodium azide **2**, aromatic aldehydes **3**, and ethyl acetoacetate **4** using ultrasonic irradiation under mild conditions. The optimum conditions for the synthesis process as the catalyst amount, ultrasonic irradiation, and solvent were adjusted. The priority of its catalytic role was asserted in comparison with other recommended catalysts. The green synthesis process that was accomplished in a small time with high yield is the conclusion of ARPTPd and ultrasonic irradiation role. Also, computational studies were done to confirm or discriminate variable practical features. Crystal surface properties were obtained by using Crystal Maker, among the significant proximity of oxygen atoms to the surface which is effective in catalysis. DFT study was performed to optimize structural forms and offers essential quantum parameters. Also, the catalytic behavior of the ARPTPd catalyst was suggested and supported by DTF outcomes.

ACKNOWLEDGEMENTS

Dr. Mohamed acknowledge Taif University Researchers Supporting Project number (TURSP-2020/43), Taif University, Taif, Saudi Arabia.

CONFLICT OF INTEREST

The authors declare no conflict of interest.

AUTHOR CONTRIBUTIONS

Mahmoud Abd El Aleem Ali Ali El-Remaily: Supervision. **Ahmed M. M. Soliman:** Supervision. **Mohamed Khalifa:** Methodology. **Nashwa El-Metwaly:** Supervision. **Amerah Alsoliemy:** Methodology. **Tarek El-Dabea:** Investigation. **Ahmed Abu-Dief:**Supervision.

ORCID

Mahmoud Abd El Aleem Ali Ali El-Remaily https://orcid.org/0000-0002-3591-0077
Ahmed M. M. Soliman https://orcid.org/0000-0003-2541-638X
Mohamed E. Khalifa https://orcid.org/0000-0003-4914-4796
Nashwa M. El-Metwaly https://orcid.org/0000-0002-0619-6206
Tarek El-Dabea https://orcid.org/0000-0002-5359-6931
Ahmed M. Abu-Dief https://orcid.org/0000-0003-3771-9011

REFERENCES

[1] a) N. C. Eddingsaas, K. S. Suslick, *Nature* **2006**, *444*, 163. b) K. S. Suslick, *Science* **1990**, *247*, 1439. c) M. R. Hoffmann, I. Hua, R. Höchemer, *Ultrason. Sonochem.* **1996**, *3*, 163.
[2] N. Ghaffari Khaligh, F. Shirini, *Ultrason. Sonochem.* **2015**, *22*, 397.
[3] a) K. S. Suslick, *Sci. Am.* **1989**, *260*, 80. b) J. H. Bang, K. S. Suslick, *Adv. Mater.* **2010**, *22*, 1039.
[4] a) S. Allahyari, M. Haghighi, A. Ebadi, S. Hosseinzadeh, *Ultrason. Sonochem.* **2014**, *21*, 663. b) M. Mirza-Aghayan, N. Ganjbakhsh, M. Molaee Tavana, R. Boukherroub, *Ultrason. Sonochem.* **2016**, *32*, 37.
[5] a) A. Ramazani, M. Rouhani, S. W. Joo, *Ultrason. Sonochem.* **2016**, *28*, 393. b) J. Safaei-Ghomi, Z. Akbarzadeh, *Ultrason. Sonochem.* **2015**, *22*, 365.
[6] a) H. Xu, B. W. Zeiger, K. S. Suslick, *Chem. Soc. Rev.* **2013**, *42*, 2555. b) G. Cravotto, P. Cintas, *Chem. Soc. Rev.* **2006**, *35*, 180.
[7] a) A. Maleki, A. Sarvary, *RSC Adv.* **2015**, *5*, 60938. b) A. Sarvary, A. Maleki, *Mol. Diversity* **2015**, *19*, 189.
[8] a) A. Maleki, P. Ravaghi, M. Aghaei, H. Movahed, *Res. Chem. Intermed.* **2017**, *43*, 5485. b) X. Wang, Y. Wei, Y. Da, Z. Zhang, Z. Quan, *Heterocycles* **2011**, *83*, 2811.
[9] a) T. Li, C. Yao, C. Yu, X. Wang, S. Tu, *Syn. Commun.* **2012**, *42*, 2728. b) M. V. Goryaeva, Y. V. Burgart, M. A. Ezhikova, M. I. Kodess, V. I. Saloutin, *Russ. J. Org. Chem.* **2015**, *51*, 992.
[10] a) M. V. Goryaeva, Y. V. Burgart, M. A. Ezhikova, M. I. Kodess, V. I. Saloutin, *Beilstein J. Org. Chem.* **2015**, *11*, 385. b) O. V. Fedorova, M. S. Zhidovinova, G. L. Rusinov, I. G. Ovchinnikova, *Russ. Chem. Bull.* **2003**, *52*, 1768.
[11] a) J. Hashim, N. Arshad, I. Khan, S. Nisar, B. Ali, M. I. Choudhary, *Tetrahedron* **2014**, *70*, 8582. b) A. Yao, S. Lei, C. Wang, C. Yu, S. Tu, *J. Heterocycl. Chem.* **2008**, *45*, 1609.
[12] a) V. L. Gein, I. N. Vladimirov, O. V. Fedorova, A. A. Kurbatova, N. V. Nosova, I. V. Krylova, M. I. Vakhrin, *Russ. J. Org. Chem.* **2010**, *46*, 699. b) A. Haleel, P. Arthi, N. Dastagiri Reddy, V. Veena, N. Sakthivel, Y. Arun, P. T. Perumal, A. Kalilur Rahiman, *RSC Adv.* **2014**, *4*, 60816.
[13] V. L. Rusinov, V. N. Charushin, O. N. Chupakhin, *Russ. Chem. Bull.* **2018**, *67*, 573.
[14] A. M. Dougherty, H. Guo, G. Westby, Y. Liu, E. Simsek, J. T. Guo, A. Mehta, P. Norton, B. Gu, T. Block, A. Cuconati, *Antimicrob. Agents Chemother.* **2007**, *51*, 4427.
[15] A. M. Hussein, O. M. Ahmed, *Bioorg. Med. Chem.* **2010**, *18*, 2639.
[16] A. Haleel, P. Arthi, N. D. Reddy, V. Veena, N. Sakthivel, Y. Arun, P. T. Perumal, A. K. Rahiman, *RSC Adv.* **2014**, *4*, 60816.
[17] C. Raju, K. Madhaiyan, R. Uma, R. Sridhar, S. Ramakrishna, *RSC Adv.* **2012**, *2*, 11657.
[18] A. Haleel, D. Mahendiran, V. Veena, N. Sakthivel, A. K. Rahiman, *Mater. Sci. Eng. C.* **2016**, *68*, 366.
[19] a) M. A. A. El-Remaily, O. M. Elhady, *Appl. Organometal. Chem.* **2019**, *33*, 4989. b) M. A. A. El-Remaily, O. M. Elhady, *Tetrahedron Lett.* **2016**, *57*, 435. c) M. A. A. El-Remaily, H. A. J. Hamad, *Mol. Cata. A: Chem.* **2015**, *404*, 148. d) M. A. A. El-Remaily, A. M. Abu-Dief, *Tetrahedron* **2015**, *71*, 2579. e) M. A. A. El-Remaily, *Tetrahedron* **2014**, *70*, 2971. f) M. A. A. El-Remaily, *Chin. J. Cata* **2015**, *36*, 1124. g) M. A. A. El-Remaily, A. M. M. Soliman, O. M. Elhady, *ACS Omaga* **2020**. h) A. M. M. Soliman, S. K. Mohamed, M. A. A. El-Remaily, H. Abdel-Ghany, *Eur. J. Med. Chem.* **2012**, *47*, 138. i) M. A. A. El-Remaily, A. M. M. Soliman, *Chem* **2016**, *37*, 70. j) M. A. A. El-Remaily, O. M. Elhady, *Chemistry Select* **2020**, *5*(39). k) E. A. Ahmed, A. M. M. Soliman, A. M. Ali, M. A. A. El-Remaily, *Appl. Organometal. Chem.* **2021**, *35*. https://doi.org/10.1002/aoc.6197 l) M. A. A. El-Remaily, H. A. Hamad, O. M. Elhady, *Appl. Organometal. Chem* **2021**, *35*. https://doi.org/10.1002/aoc.6238 m) E. K. Shokr, M. S. Kamel, H. Abdel-Ghany, M. A. A. El-Remaily, *Curr. Res. Green Sustain. Chem.* **2021**, *4*, 100090. n) H. A. Hamad, H. Nageh, H. M. El-Bery, A. Kasry, F. Carrasco-Marín, O. M. Elhady, A. M. M. Soliman, M. A. A. El-Remaily, *J. Colloid Interface Sci.* **2021**, *599*, 227.
[20] a) S. O. Alzahrani, A. M. Abu-Dief, K. Alkhamis, F. Alkhatib, T. El-Dabea, M. A. A. El-Remaily, N. M. El-Metwaly, *J. Mol. Liqs.* **2021**, *332*, 115844. b) H. S. Sun, J. Q. Wang, C. Guo, L. J. Shen, *Chin. J. Org. Chem.* **2013**, *33*, 2220. c) A. M. Abu-Dief, N. M. El-Metwaly, S. O. Alzahrani, F. Alkhatib, M. M. Abualnaja, T. El-Dabea, M. A. A. El-Remaily, *J. Mol. Liq.* **2021**, *326*, 115277.
[21] a) H. M. Abd El-Lateef, A. M. Abu-Dief, M. A. A. Mohamed, *J. Mol. Struct.* **2017**, *1130*, 522. b) H. M. Abd El-Lateef, A. M. Abu-Dief, B. E. D. M. El-Gendy, *J. Electroanal. Chem.* **2015**. c) H. M. Abd El-Lateef, A. M. Abu-Dief, L. H. Abdel-Rahman, E. C. Sañudo, N. Aliaga Alcalde, *J. Electroanal. Chem.* **2015**, *743*, 120.
[22] a) L. H. Abdel-Rahman, A. M. Abu-Dief, M. Basha, A. A. H. Abdel-Mawgoud, *Appl. Organometal. Chem.* **2017**, *31*, 3750. b) L. H. Abdel-Rahman, A. M. Abu-Dief, M. Ismael, M. A. A. Mohamed, N. A. Hashem, *J. Mol. Struct.* **2016**, *1103*, 232.
[23] W. Coats, J. P. Redfern, *Nature* **1964**, *201*, 68.
[24] E. S. Freeman, B. Carroll, *J. Phys.Chem.* **1958**, *62*, 394.
[25] G. A. Bain, J. F. Berry, *Chem. Educ.* **2008**, *85*, 532.
[26] P. Kofstad, *Oxidation of Metals: Nature* **1957**, *179*, 1362.
[27] J. H. F. Flynn, L. A. Wall, *J. Res. Natl. Bur. Stand. A.* **1966**, *70*, 487.
[28] W. W. Wendlandt, *Thermal Methods of Analysis*, Wiley, New York **1974**.
[29] T. Ozawa, *Bull. Chem. Sot. Japan.* **1965**, *38*, 1881.
[30] H. W. Horowitz, G. A. Metzger, *Anal. Chem.* **1963**, *35*, 1464.
[31] a) A. Yao, S. Lei, C. Wang, C. Yu, S. Tu, *J. Heterocycl. Chem.* **2008**, *45*, 1609. b) V. L. Gein, I. N. Vladimirov, O. V. Fedorova,

A. A. Kurbatova, N. V. Nosova, I. V. Krylova, M. I. Vakhrin, *Russ. J. Org. Chem.* **2010**, *46*, 699.

[32] a) A. Maleki, J. Rahimi, O. M. Demchuk, A. Z. Wilczewska, R. Jasiński, *Ultrasonics - Sonochemistry* **2018**, *43*, 262. b) A. Maleki, M. Niksefat, J. Rahimi, S. Azadegan, *Polyhedron* **2019**, *167*, 103.

[33] Modeling and Simulation Solutions for Chemicals and Materials Research, Materials Studio (Version 5.0), Accelrys software Inc., San Diego, USA. Available online at: www.accelrys.com **2009**.

[34] M. J. Frisch, G. W. Trucks, J. A. Pople, *Gaussian 09, Revision B.2*, Gaussian, Inc, Pittsburgh, PA **2009**.

[35] W. J. Hehre, L. Radom, P. V. R. Schlyer, J. A. Pople, *Ab Initio Molecular Orbital Theory*, Wiley, New York **1986**.

[36] A. Kessi, B. Delley, *Int. J. Quantum Chem.* **1998**, *68*, 135.

[37] W. J. Geary, *Coordin. Chem. Rev.* **1971**, *7*, 81.

[38] a) A. M. Abu-Dief, N. M. El-Metwaly, S. Omar Alzahrani, A. M. Bawazeer, S. Shaaban, M. Shaker, S. Adam, *J. Mol. Liquids* **2020**. (b) A. M. Abu-Dief, N. M. El-Metwaly, S. O. Alzahrani, F. Alkhatib, H. M. Abumelha, T. El-Dabea, M. A. A. El-Remaily, *Res. Chem. Intermed.* **2021**, *47*, 1979.

[39] G. A. A. Al-Hazmi, K. S. Abou-Melha, N. M. El-Metwaly, I. Althagafi, F. Shaaban, R. Zaky, *Appl Organometal Chem.* **2020**, *34*, e5403.

[40] L. H. Abdel-Rahman, A. M. Abu-Dief, H. Moustafa, A. A. Hassan Abdel-Mawgoud, *Arabian J. Chem* **2020**, *13*(1), 649.

[41] a) L. H. Abdel-Rahman, A. M. Abu-Dief, H. Mostafa, S. K. Hamdan, *Appl. Organometal. Chem.* **2017**, *31*, e3555.

[42] G. Al-Hazmi, K. Abou-Melha, N. El-Metwaly, I. Althagafi, F. Shabaan, R. Zaky, *Appl Organometal Chem.* **2019**, e540.

[43] G. R. Reddy, S. Balasubramanian, K. Chennakesavulu, *J. Mater, Chem. A* **2014**, *2*, 15598.

[44] a) A. Bean Getsoian, Z. Zhai, A. Bell, *J. Am. Chem. Soc.* **2014**, *136*(39). b) N. F. Mott, E. A. Davis, *Electrochemical Process In Non-crystalline Materials*, Calendron Press, Oxford **1979**.

[45] F. A. Saad, J. H. Al-Fahemi, H. El-Ghamry, A. M. Khedr, M. G. Elghalban, N. M. El-Metwaly, *J. Therm. Anal. Calorim.* **2018**, *131*(2).

[46] F. A. Saad, M. G. Elghalban, J. H. Al-Fahemi, N. Yarkandy, N. M. El-Metwaly, K. S. Abou-Melha, G. A. Al-Hazmi, K. A. Saleh, *J. Therm. Anal. Calorim.* **2017**, *128*(3), 1565.

[47] H. Katouah, A. M. Hameed, A. Alharbi, F. Alkhatib, R. Shah, S. Alzahrani, R. Zaky, N. M. El-Metwaly, *ChemistrySelect* **2020**, *5*, 10256.

[48] A. M. Abu-Dief, L. H. Abdel-Rahman, M. R. Shehata, A. A. H. Abdel-Mawgoud, *J. Phys. Org. Chem.* **2019**, *32*(12).

[49] L. H. Abdel-Rahman, M. S. S. Adam, A. M. Abu-Dief, H. Moustafa, M. T. Basha, A. S. Aboraia, B. S. Al-Farhan, H. E. Ahmed, *Appl. Organometal. Chem* **2018**.

[50] S. Bräse, K. Banert, *Organic Azides Syntheses and Applications*, John Wiley & Sons, Hoboken **2009**.

[51] M. J. Turner, J. J. McKinnon, D. Jayatilaka, M. A. Spackman, *Cryst. Eng. Comm.* **2011**, *13*, 1804.

[52] K. Momma, F. Izumi, *J. Appl. Crystallogr.* **2011**, *44*, 1272.

[53] M. Daturi, L. Savary, G. Costentin, J. Lavalley, *Catal. Today* **2000**, *61*, 231.

[54] R. Shah, H. Katouah, A. A. Sedayo, M. Abualnaja, M. M. Aljohani, F. Saad, R. Zaky, N. M. El-Metwaly, *J. Mol. Liquids* **2020**, *319*.

[55] a) L. O. Olasunkanmi, I. B. Obot, E. E. Ebenso, *RSC Adv.* **2016**, *6*. b) F. A. La Porta, T. C. Ramalho, R. T. Santiago, M. V. J. Rocha, E. F. F. da Cunha, *J. Phys. Chem. A* **2011**, *115*, 824.

[56] a) A. S. Al-Wasidi, N. M. Al-Jafshar, A. M. Al-Anazi, M. S. Refat, N. M. El-Metwaly, H. K. Ibrahim, W. Abd El-Fattah, A. M. Naglah, M. A. Al-Omar, A. Kalmouch, *Sci. Adv. Mater. 12*(8), 1137. b) E. P. da Rocha, H. A. Rodrigues, E. F. F. da Cunha, T. C. Ramalho, *Comput. Theor. Chem.* **2016**, *1096*, 17.

[57] a) S. Y. Al-nami, E. Aljuhani, I. Althagafi, H. M. Abumelha, T. M. Bawazeer, A. M. Al-Solimy, Z. A. Al-Ahmed, F. Al-Zahrani, N. El-Metwaly, *Arabian J. Sci. Eng.* 1. b) R. R. da Silva, T. C. Ramalho, J. M. Santos, J. Daniel Figueroa-Villar, *J. Phys, Chem. A* **2006**, *110*, 1031.

[58] Z. El Adnani, M. Mcharfi, M. Sfaira, M. Benzakour, A. Benjelloun, M. E. Touhami, *Corros. Sci.* **2013**, *68*, 223.

[59] a) M. Frisch, G. Trucks, H. Schlegel, G. Scuseria, M. Robb, J. Cheeseman, G. Scalmani, V. Barone, B. Mennucci, G. Petersson, *Gaussian 09, Revision A. 1*, Wallingford, CT, USA, Gaussian **2009**. b) Y. Zhao, *D. G. Truhlar. Theor. Chem. Acc.* **2008**, *120*, 215. c) J.-D. Chaia, M. Head-Gordon, *Phys. Chem. Chem. Phys.* **2008**, *10*, 6615. d) A. J. Garza, G. E. Scuseria, *J. Physical Chem, Lett.* **2016**, *8*, 380. e) N. Mardirossian, M. Head-Gordon, *Mol. Phys.* **2017**, *115*, 2315. (f)L. Goerigk, A. Hansen, C. Bauer, S. Ehrlich, A. Najibi, S. Grimme, *Phys. Chem. Chem. Phys.* **2017**, *19*, 32184.

SUPPORTING INFORMATION

Additional supporting information may be found online in the Supporting Information section at the end of this article.

How to cite this article: M. A. E. A. A. A. El-Remaily, A. M. M. Soliman, M. E. Khalifa, N. M. El-Metwaly, A. Alsoliemy, T. El-Dabea, A. M. Abu-Dief, *Appl Organomet Chem* **2021**, e6320. https://doi.org/10.1002/aoc.6320